Published in IET Science, Measurement and Technology
Received on 6th June 2007
Revised on 5th September 2008
doi: 10.1049/iet-smt:20080091

Special Issue – selected papers from CEM 2008

ISSN 1751-8822

Finite-element assisted method to reduce harmonic content in the air-gap flux density of a high-temperature superconducting coreless rotor generator

B. Lukasik K.F. Goddard J.K. Sykulski

School of Electronics and Computer Science, University of Southampton, Southampton SO17 1BJ, UK
E-mail: jks@soton.ac.uk

Abstract: An investigation to reduce harmonic content in the air-gap flux density of a high-temperature superconducting synchronous generator with a coreless rotor is reported. Three-dimensional finite-element field simulation has been used to predict the voltage waveform of the machine. A simple technique was applied to guide the design process. This allowed the waveform to be improved using a small number of finite-element models.

1 Introduction

Although the demand for electrical energy is constantly increasing, it becomes practically impossible to build bigger conventional machines (because of size, weight limitations and material strength). Recent advances in high-temperature superconducting (HTS) materials allow them to carry much higher current densities which may overcome these limits [1, 2]. Alternatively, the higher current densities may be used to reduce the size of the machine for similar rating. The higher current density also, in principle, makes it possible to build a machine without a magnetic core because in the same volume, it is able to produce enough air-gap flux density. HTS generators are a relatively new application for these novel materials. However, despite their superiority in many aspects, HTS materials also pose some new difficulties. Therefore the successful design of such novel machines requires a very careful design process. This helps to identify possible problems. Because of the constantly increasing performance of computers, it is now possible to accurately model and optimise such new devices using commercially available finite-element packages.

2 Design of a generator with a coreless rotor

This paper reports on challenges faced during the design of an HTS generator with a coreless rotor currently being built at the University of Southampton. The project focuses on building a superconducting coreless generator using a second generation superconducting (BSCCO) tape. It is a direct descendant of the previous project completed at Southampton when a cored generator was successfully designed, built and tested [3]. The principle objectives are to build a superconducting synchronous generator with a coreless rotor, minimise its mass and maximise its performance. The HTS material chosen for the device unfortunately requires retaining some magnetic material in the rotor to control magnetic field distribution.

As in the previous project, in order to reduce the costs, the stator was taken from a conventional 100 kVA, two-pole induction machine, with the bore diameter of 330 mm and iron length of 325 mm. A short-pitched (14/24) two-layer winding with three-turn coils is distributed in 48 slots and connected in a parallel star arrangement. Using an existing stator introduced additional constraints on the design, in

particular regarding the control of higher harmonics in the voltage waveform.

2.1 Rotor

The rotor of the machine is designed to be of the coreless type, that is, there is no magnetic core. This makes the required magnetising current much higher when compared with classical, cored, designs. It also increases the magnetic field in the superconducting coils. In order to limit the field perpendicular to the broad face of the tape, a set of flux diverters have been introduced (as in previous designs [3, 4]). These are 9% nickel steel rings placed above each coil to divert the magnetic field around the coils. This material was chosen because it is suitable for low temperatures and has a high saturation flux density. In the preliminary designs, the rotor had 24 coils. However, the minimum bend radius (38 mm) of the tape and other mechanical constraints ultimately forced the removal of the three top coils. The removed coils allowed for a bigger top diverter which created more design freedom for shaping of the flux waveform. Unfortunately, the mechanical considerations required the through bolts to be added in order to hold the whole rotor assembly together. This required the top hat material to be changed to Invar, since the structural integrity of the rotor became heavily reliant on this component. In the modified design, the field winding has eighteen 60-turn coils. Each of the coils is placed in a fibreglass former spanning across the whole rotor width. Every former has a pocket for a coil and is placed between and supports the flux diverters. Each of the diverter rings has been made to have a 3 mm overhang on the inside and outside of the coil, to keep most of the fringing flux out of the HTS coils. The whole stack is placed in a stainless steel tube lined with copper to shield the interior of the rotor from stator mmf (magneto motive force) harmonics. The tube is a cold vessel flooded with liquid nitrogen to cool the coils and the copper layer. The preliminary rotor arrangement and the shape of diverters are shown in Fig. 1. As can be seen, the rotor configuration was chosen to follow the curvature of the enclosing stainless steel tube in order to maximise the coil area hence maximising the air-gap flux density. The fundamental component should not fall below 0.5 T. The design proposed and described later in this paper has a maximum value of air-gap flux density equal to 0.54 T.

2.2 Design considerations and constraints

Superconducting machines set new constraints that must be met before a successful device can be built. These include providing appropriate working conditions for the HTS winding, limiting the load on the refrigeration system and accommodating thermal contraction.

The superconducting tape (BSCCO) used in the project is rated at 180 A. Its anisotropic properties require very careful design of the rotor in order to accommodate the constraints imposed by the material. To ensure sufficient critical current in the superconductor at the proposed working temperature of 66 K, the magnetic field both in parallel and perpendicular directions to the broad face of the tape must be kept under acceptable limits. For the tape used in the current project, the limiting flux densities are 1.5 T for the parallel field ($B_{\parallel}$) and 0.13 T for the field perpendicular ($B_{\perp}$) to the broad face of the tape.

The voltage waveform is of primary concern when a successful machine needs to be built. A high harmonic content would deem the machine unusable in electrical networks. The ideal outcome is not to have any harmonics in the output voltage but, since this is not possible in practice, the designer needs to focus on reducing them to the minimum. The output voltage harmonic content depends on the configuration of the stator winding and the air-gap flux density waveform produced by the field winding. As mentioned before, the stator has been taken from an existing machine; therefore no improvement is possible there. All the modifications must be restricted to the design of the rotor.

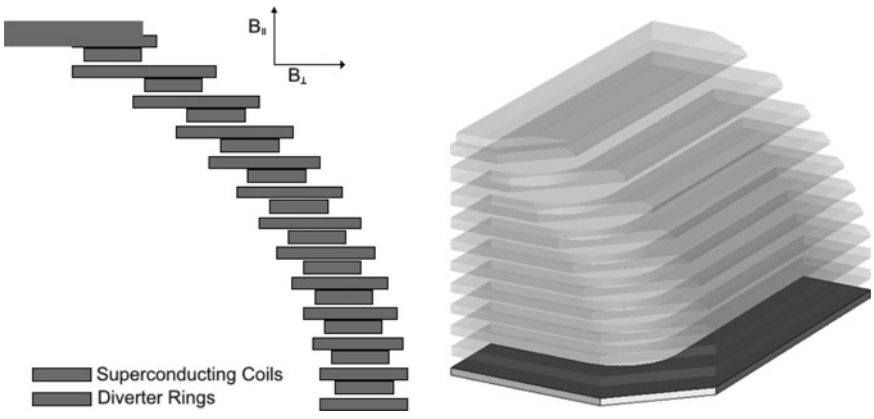

Figure 1 *Stack of diverters and coils is shown on the left as a cross-section of the rotor*
The picture on the right provides a 3D view (with only one-eighth of the rotor shown because of symmetry)

doi: 10.1049/iet-smt:20080091

The other electromagnetic constraint that needs to be addressed in a successful design of such a machine is losses in the cold part of the rotor, mainly caused by eddy currents, since these can impose a significant load on the cooling system.

The thermal requirements complicate the mechanical design considerably. The structure that supports the mass of the rotor must limit the heat leak into the cold part of the machine, while also being sufficiently stiff to keep the critical speeds of the rotor out of the working range.

The proposed design has 9% nickel rings, two Invar diverters (top and bottom), fibreglass formers, superconducting coils, stainless steel bolts and a stainless steel outer can. These materials have a wide range of contraction coefficients. The successful design, however, must ensure that the whole assembly is held together properly at low temperatures and high speeds, which are normal operating conditions for the machine. The lack of a magnetic core – which from the mechanical point of view provided a very good structural support – introduces additional difficulties. When all the material parameters and all the stresses are analysed, it becomes obvious that the solution is not that straightforward. All these constraints ultimately lead to many changes in the mechanical design which interfered with the process of improving electromagnetic performance of the machine.

3 Minimisation of harmonic distortion

When a classical optimisation process is considered, it involves defining an objective function dependent on a number of variables. The optimiser then explores the space of the function and typically looks for appropriate gradients of the parameters defined in the function. Then, it decides to follow a certain direction which the algorithm evaluates to have the highest chance to meet the objective. When further improvement is not possible, the algorithm evaluates the objective function gradients from the point it reached at the last step.

Such a process may be computationally expensive and when the model itself is complicated, the computational costs rise enormously. In our case, the features of the machine require the use of 3D models, each requiring between 4.5 and 5.5 million elements. Each solution takes ~90 h on a 64-bit Linux server and requires 6 GB of RAM. Most of the time (nearly 90%) is taken by the calculation of coil fields prior to the solution of simultaneous equations. In comparison, post-processing requires only 2 h. Using such computationally expensive models to explore search space and evaluate gradients of the objective function would be impractical.

To identify beneficial modifications, a simple formula, first suggested in [5], was used. It provides a very good guidance for improving the rotor shape with the aim to minimise the harmonic content in the air-gap flux density waveform using

$$\frac{\partial V_i^2}{\partial B_{\mathrm{r}}(\theta)} = 2V_i \frac{\partial V_i}{\partial B_{\mathrm{r}}(\theta)} \tag{1}$$

and applying the quotient rule yields

$$\frac{\partial}{\partial B_{\mathrm{r}}(\theta)}\left(\frac{\sum_{i>1} V_i^2}{V_1^2}\right) = \left(\frac{2}{V_1^2}\right)\left[\sum_{i>1}\left(V_i \frac{\partial V_i}{\partial B_{\mathrm{r}}(\theta)}\right) - \left(\frac{\sum_{i>1} V_i^2}{V_1^2}\right)\left(V_1 \frac{\partial V_1}{\partial B_{\mathrm{r}}(\theta)}\right)\right] \tag{2}$$

where V_1 is the fundamental harmonic, V_i the ith harmonic of the voltage and B_{r} the radial flux density in the air gap with the other symbols having the usual meaning.

This function gives the designer a very good estimate of which parts of the rotor should have the flux increased (by adding more ampere-turns or iron) and where it should be reduced. Thus, it allows the designer to control the process and so helps to significantly reduce the number of iterations required for minimising the harmonic content. The method can be used with any type of a model, but requires that the derivative of the objective function with respect to the air-gap flux density can be estimated without the use of computationally expensive models. The values of $\partial V_i/\partial B_{\mathrm{r}}(\theta)$ were estimated by assuming that any additional radial flux would flow through the nearest stator tooth, and links stator coils accordingly. The accuracy of these estimates is less critical than that of the estimates of the voltage harmonics themselves, since the changes made in any single iteration are generally small.

4 Types of finite-element models and their limitations

4.1 2D models

Two-dimensional finite-element models are easy to build and to post-process, and require much less computation than 3D models. The lower computational cost makes the use of automatic optimisation routines much more practical. However, the reduced cost is achieved at the expense of reduced accuracy.

In addition to 2D models based on the infinite-length approximation, axi-symmetric and axi-harmonic model types may also be available. However, these types of models are clearly not applicable to the type of machine considered here and will not be considered further.

It is possible to improve the accuracy of 2D models by connecting them to external circuits with additional

end-winding inductances. However, to obtain suitable values for these inductances, either 3D models or empirical formulae are required. Empirical formulae require validation for a wide range of design variants; for a conventional design, it may be possible to do this by reference to previous work, but this is unlikely to be possible for a novel design. Use of 3D models to obtain values of end-winding inductances would be advantageous only if the same models could be used for a large number of design variants. Moreover, for the configuration of the machine considered here, there are additional flux paths across the ends of the flux diverter rings that cannot be represented in 2D model or be included in the external circuit.

In addition to the types of models discussed above, 2D transient rotating machine solvers are now widely available. Since these formulations are inherently transient, they are computationally much more expensive than static or steady-state AC models. Moreover, in an ordinary transient analysis, it is possible to extend the length of the time steps as the fast transients die away, whereas frequent slot-passing events prevent this in a rotating machine analysis. Although rotating-machine models are useful for estimating the eddy-current losses on the rotor, they do not improve the accuracy of the output waveform predictions sufficiently to justify their relatively high cost.

4.2 3D models

As noted above, 2D finite-element models cannot give reliable estimates of the output waveform of a generator with an unconventional configuration such as that considered here. The use of some form of 3D modelling is therefore essential. The least computationally expensive option is to use a static model. Obviously, in a static model, eddy currents are neglected. Since the rotor contains a copper eddy-current screen to shield the flux diverters from the field of the stator mmf harmonics, including these harmonics in a static model is not appropriate. Instead, their effects should be modelled separately. If, in addition to the static solution, a series of steady-state AC solutions are obtained, the transient characteristics of the machine can also be estimated [6].

In principle, the software we used allows development of a full 3D rotating machine model. However, the computational costs involved are so high that use of such models for optimisation becomes completely impractical.

In addition to the choice of solution types, the 3D finite-element package that we are using offers a choice of different types of winding representations. 'Circuit windings' are represented by a series of small (mesh size) current filaments and are placed in regions of total vector potential. This allows the program to obtain the flux linkage from $\int A \cdot \mathrm{d}l$. In principle, the use of this type of winding should allow the output voltage waveform to be obtained from the circuit results without any need for integrating the fields predicted by the model. However, the software seems to be unreliable when building a model with this type of the stator winding, and usually fails with an error message that does not help to locate the problem. Hence the use of this type of winding had to be rejected. It should be noted that this type of winding is required for a 3D rotating machine analysis; hence – even if the computational costs were acceptable – this option would also have to be rejected.

Instead, the windings are built from current-source conductors. These can be defined independently of the mesh, so that they do not cause problems in building the model. However, the current-source conductors must be placed in regions of reduced potential; hence flux linkage cannot be obtained from $\int A \cdot \mathrm{d}l$. Making the mesh independent of the conductor geometry introduces some post-processing errors if nodal interpolation of coil fields is used. Meshed current-source conductors may be mixed with the mesh-independent type to reduce these errors, but use of this type of conductor also seems to increase the risk of the program failing to build the model.

4.3 Modelling the stator winding

The stator winding consists of 24 pairs of coils, each formed from a number of conductors with a rectangular cross-section. Originally, these were all modelled as 8- or 20-node brick conductors. Constructing the coil using only brick conductors simplifies the problem of matching adjacent ends. A number of brick conductors were later replaced by a smaller number of straight or arc conductors, since this reduced the amount of time required for the solver to calculate the coil fields. However, since the majority of the brick conductors could not be replaced in this way, the savings are not large.

The centre line of the conductors was first determined in $r-z$ coordinates, using common tangent calculations. The angular position of the arc conductors was fixed with the angular position of the knuckle midway between the two slots that carry the straight conductors. The bulk of the end winding follows two helical paths. The ends of these sections are located so that, if extended by $\sim$8 mm, they would come to a point 8 mm along the tangent from the ends of the arcs that they are to be connected to. The 8 mm dimension was considered suitable in relation to the 8 mm $\times$ 16 mm rectangular cross-section of the conductors.

Tangential unit vectors were calculated at the points along the curves corresponding to the ends of the 20-node brick conductors that form these sections of the winding. These unit vectors define the normal to the rectangular end faces of the conductors. To simplify these calculations, the helical curves had uniform values of $\mathrm{d}r/\mathrm{d}\theta$ and $\mathrm{d}z/\mathrm{d}\theta$. Next, an orthogonal vector in the local $r-z$ plane was defined for each point, and the cross product with the original unit vector was formed. The two new vectors define the orientation of the rectangle where adjacent

doi: 10.1049/iet-smt:20080091

conductors meet. The mid-side nodes that do not lie on the rectangular end faces are located by taking the mean position of the associated corners and applying an adjustment based on the distance between the end points and the tangential vectors at the two end faces. The adjustment is given by $l\,(t_1 - t_2)/(6.65 + 1.37 * t_1 \cdot t_2)$, where t_1 and t_2 are the two tangential unit vectors, and l is the distance between the two ends of the line. The two constants are chosen to approximate the correct area under an arc for a range of angles from 0° to 90°.

4.4 Extracting stator flux linkage values

The stator winding is 'built' (modelled) out of current-source conductors. This type of conductor was chosen since it does not complicate the meshing of the model. Thus, models are easier to build and less likely to require further work to avoid errors associated with meshing. However, when using current-source conductors, the whole coil must be placed in a simply connected volume of reduced potential. Since the coils occupy regions of reduced potential, it is not possible to calculate the flux linking a coil from the values of vector potential in the coil. Instead, the flux linkage must be calculated from values of B extracted from the 3D model at a large number of positions. The flux linking each coil was estimated from integrals of the normal component of B over a large number of eight-node quadrilateral patches. These patches were arranged into six sets, such that each set formed a continuous surface with its outer edges following a current streamline within the coil. These six paths were uniformly distributed over the cross-section of the conductor and were defined using data generated while building the stator winding.

To avoid discontinuities in B, which would reduce the accuracy of the integration, two patches are used for each path in each stator conductor. The one that has an edge within the conductor has two radial edges extending to a radius within the air gap with the mid-side node of the fourth edge at the same radius with θ and z coordinates that are the average of the two corner points. The second patch shares this edge, whereas the opposite edge has the same r and z coordinates but has θ equal to that of the knuckle; the other two mid-side nodes are placed on the same cylindrical surface with the same z as the corresponding end points. Although it would have been simpler to use a four-node cylindrical patch, this would not exactly match at the shared edge. Three different radii were used for the patches in the air gap, each being used for two of the current paths; this was done to minimise numerical errors.

5 Results

The objective of the design was to minimise the harmonic content without unduly increasing the mass of the rotor or reducing the output voltage of the generator. The first two shapes presented in Fig. 2 were taken directly from the 2D models. The one presented in Fig. 2*a* shows two top diverters. In the preliminary designs, there was an extra coil between them which was later removed because of mechanical considerations. The second shape presents the diverter that replaced the previous two. It can be seen that it has no clamping bolts. The whole rotor assembly was supposed to be held together by an external stainless steel tube. Unfortunately, this arrangement proved to be very hard to implement and that required the clamping bolts to be introduced. There were 12 envisaged initially but the final number was decided to be 14. In addition to that, the material of the top-most diverter had to be changed to Invar as it has enough toughness at the temperatures below 73 K. These frequent changes interfered with the process of reducing waveform harmonics which would otherwise have been able to steadily converge to the best solution. The

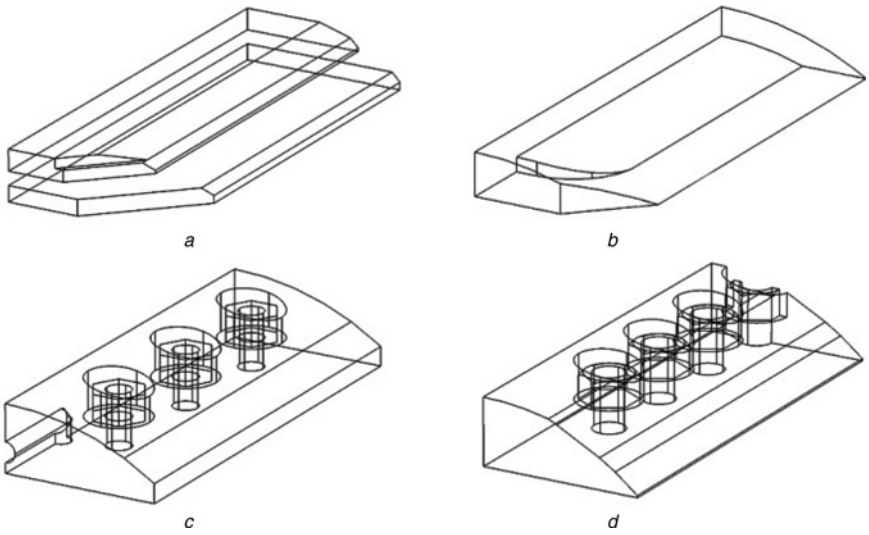

Figure 2 *Different shapes of the top-most diverter showing the progression of the design. The changes from a to b and from c to d were determined using the technique described in Section 3, while the change from b to c was made for mechanical reasons*

doi: 10.1049/iet-smt:20080091

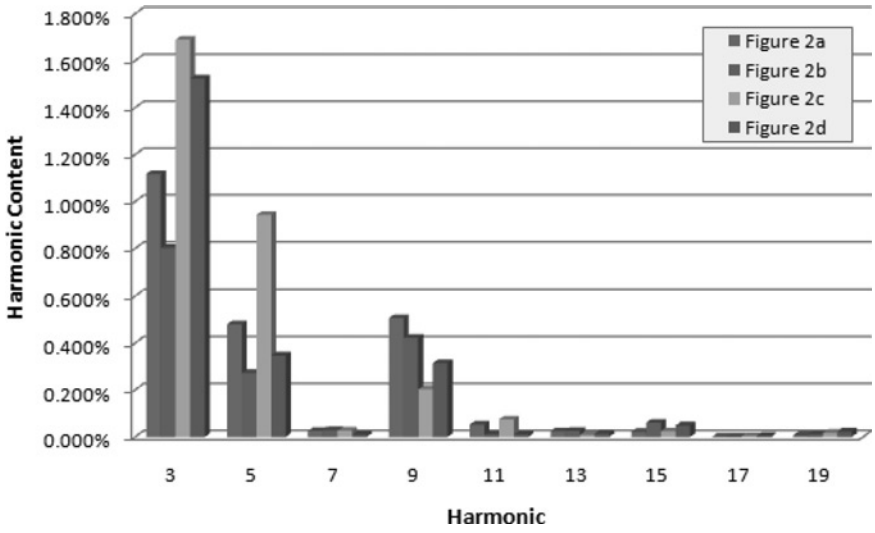

Figure 3 *Harmonic contribution for various shapes of the top-most diverter*

harmonic content for various shapes is presented in Fig. 3. As can clearly be seen, despite frequent – unwelcome but necessary – changes in the design, it was possible to improve the performance. Obviously, not all the design steps are presented here but the number of iterations required to achieve these results was not great. The minimisation of the harmonic content by using an automatic optimiser would have had a very high computational cost because of the number of models used to estimate the gradients. Frequent changes to the configuration would have made the process start all over again after each change, which would have multiplied the cost of making initial estimates of the gradients, thus further contributing to the impracticability of whole process.

The derivative of the total harmonic distortion (THD) plotted in Fig. 4 is given by

$$\text{Derivative of THD} = \frac{1}{\mathrm{d}\theta}\,\frac{0.5}{\text{THD}}\,\frac{\partial}{\partial B(\theta)}\left(\frac{\sum V_i^2}{V_1^2}\right) \qquad (3)$$

where the third factor is obtained by using (2). It can be clearly seen that the content of harmonics has been successfully reduced.

The angle 0 refers to the horizontal mid-plane of the rotor, whereas 90 is the position of the vertical mid-plane. For example, the graphs show that there is not enough flux in the lower part of the rotor, whereas there is too much at around 65°. Fig. 5 shows the cross-section of the rotor and

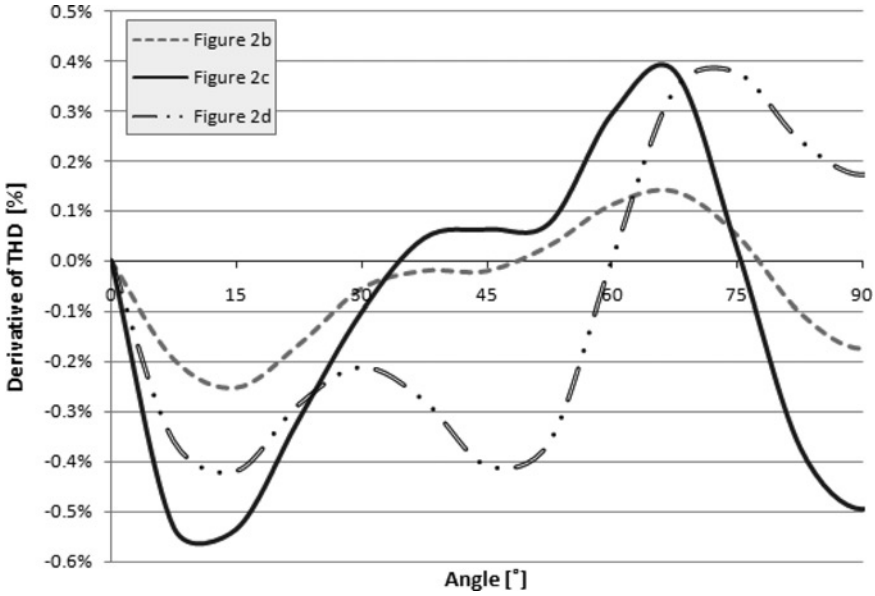

Figure 4 *Derivative of THD – $d\theta$ is in degrees, and it is assumed that similar changes in B occur in the other quadrants of the machine*

IET Sci. Meas. Technol., 2008, Vol. 2, No. 6, pp. 485–492

doi: 10.1049/iet-smt:20080091

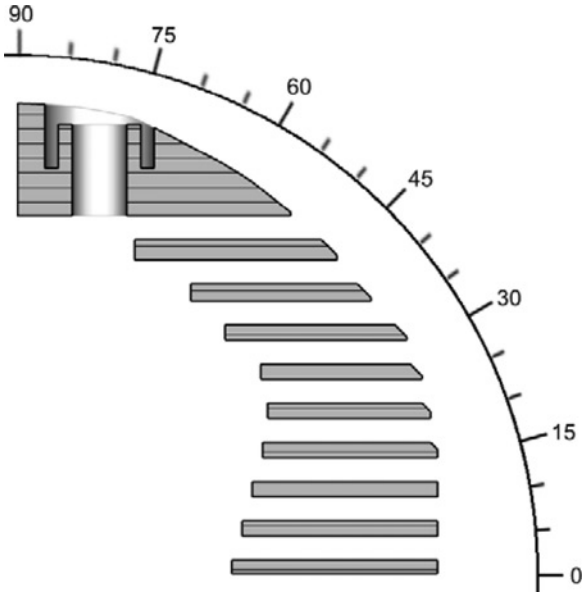

Figure 5 *Cross-section of the final shape of the rotor with the angle scale*

the appropriate angle scale. Fig. 4 shows that there are a number of areas where we might seek further improvement. Increasing the width of the lower rings and coils would increase the flux density at low angles, but supporting them would then become difficult and it is likely that the top former would be over stressed. Increasing the number of turns in the lower coils would also increase the flux density at low angles and would not cause mechanical problems, but would increase the values of $B_{\|}$ in the modified coils. Increasing the width of the ring below the top coil would increase the flux density around 45°, but the ring would probably saturate, thus increasing $B_{\perp}$ in the top two coils where it is already fairly high. One area where further modification could have improved the waveform is the top-most diverter. However, it would not be possible to remove significantly more iron from the region above the top coil because this might lead to saturation preventing the top-most diverter from effectively re-directing the flux around the top-most coil. Removing iron from the top of the rotor or using non-magnetic nuts would avoid this problem, but would have the greatest negative effect on the fundamental component of the air-gap flux density. The need for the designer to consider such constraints is a limitation of the method. Unfortunately, a similar level of guidance cannot be offered with respect to the constraints, since they are not easily related to the air-gap flux density.

Fig. 3 shows the results for the harmonic content for each of the shapes presented in Fig. 2. As the design evolved from the configuration shown in Fig. 2*a* to that in Fig. 2*b*, the THD was reduced from 1.28% to 0.93%. This was the lowest level of harmonic distortion achieved by any of the designs considered, which is not surprising as fewer mechanical constraints were considered. Fig. 3 also shows that the change of the top-most diverter and insertion of the through bolts as shown in Fig. 2*c* introduced a lot of new harmonics into the design which increased the THD to 1.89%. Although the final shape (Fig. 2*d*) required more bolts, thanks to the technique described above, it was possible to reduce the THD to 1.55%. It can be seen that the major role is played by the third harmonic and then fifth and ninth. The optimisation process of the last shape managed to reduce significantly the fifth harmonic, although increasing slightly the ninth.

6 Conclusion

The paper has addressed practical issues arising when refining the design of a generator with an HTS coreless rotor to improve its electromagnetic performance. The emphasis was on developing computational models which would allow a real design to be completed and would account for peculiar features and constraints of the machine. This was achieved by a series of compromises and approximations. The challenges faced were partly imposed by external constraints (related to mechanical and thermal requirements), partly by the complexity of the device and thus inability of the software to cope with considerable modelling demands. The project was driven by the requirement to reduce the computational cost of the whole design process.

7 Acknowledgment

The project to design, build and test an HTS generator with a coreless rotor is supported by the EPSRC grant EP/D000688/1.

8 References

[1] BARNES P.N., SUMPTION M.D., RHOADS G.L.: 'Review of high power density superconducting generators: present state and prospects for incorporating YBCO windings', *Cryogenics*, 2005, **45**, (10–11), pp. 670–686

[2] KALSI S.S., WEEBER K., TAKESUE H., LEWIS C., NEUMUELLER H.W., BLAUGHER R.D.: 'Development status of rotating machines employing superconducting field windings', *Proc. IEEE*, 2004, **92**, (10), pp. 1688–1704

[3] MOSAWI M.K., BEDUZ C., GODDARD K.F., *ET AL.*: 'Design of a 100 kVA high temperature superconducting demonstration synchronous generator', *Physica C*, 2002, **372–376**, (P3), pp. 1539–1542

[4] SYKULSKI J.K., GODDARD K., STOLL R.L.: 'High temperature superconducting demonstrator transformer: design considerations and first test results', *IEEE Trans. Magn.*, 1999, **35**, (5), pp. 3559–3561

[5] SHIP K.S., SYKULSKI J.K., GODDARD K.F.: 'Field optimisation in a synchronous generator with high temperature superconducting field winding and magnetic core', *IEE Proc., Sci. Meas. Technol.*, 2002, **149**, (5), pp. 194–198

[6] LUKASIK B., GODDARD K.F., SYKULSKI J.K.: 'Finite element assisted method of estimating equivalent circuit parameters for a superconducting synchronous generator with a coreless rotor', *IEEE Trans. Magn.*, (Accepted for publication)

doi: 10.1049/iet-smt:20080091